

# Robust Trajectory Tracking of Autonomous Surface Vehicle via Lie Algebraic Online MPC

Yinan Dong, Ziyu Xu, Tsimafei Lazouski, Sangli Teng, and Maani Ghaffari

**Abstract**—Autonomous surface vehicles (ASVs) are influenced by environmental disturbances such as wind and waves, making accurate trajectory tracking a persistent challenge in dynamic marine conditions. In this paper, we propose an efficient controller for trajectory tracking of marine vehicles under unknown disturbances by combining a convex error-state MPC on the Lie group augmented by an online learning module to compensate for these disturbances in real time. This design enables adaptive and robust tracking control while maintaining computational efficiency. Extensive evaluations in the Virtual RobotX (VRX) simulator, and real-world field experiments demonstrate that our method achieves superior tracking accuracy under various disturbance scenarios compared with existing approaches.

## I. INTRODUCTION

The autonomous surface vehicle (ASV) has played an increasingly important role in the application of marine robots, undertaking a wide range of tasks such as hydrographic surveying, environmental monitoring, and water-quality samplings [1]. For surface vehicles, the time-varying hydrodynamic coefficients and external disturbances pose an obstacle to the controller's trajectory-tracking ability, especially for underactuated ASV [2]. For example, winds, waves, currents, and inaccurate dynamics modeling can all disturb accurate tracking trajectory [3], which can lead to undesired consequences such as grounding, collision risks, or potential structural damage to the hull, thereby degrading reliability and operational safety.

Classical controllers like PID have been applied on marine robots [2], however, their performance is constrained under strong nonlinearities and time-varying disturbances. In contrast, Model Predictive Control (MPC) has demonstrated effectiveness in trajectory tracking, particularly in more complex environments [4] [5]. However, the non-linear hydrodynamics characteristics mean that the computation load of real-time MPC is heavy, resulting in a long response time to control signals, and a low motion frequency [6]. Moreover, small computing units lack the capacity to handle such heavy workloads, while large ones consume excessive space and energy, making them impractical for a compact ASV.

Multiple approaches have been put forward to alleviate the computational burden. In [7], MPC with projection neural network performs efficient constrained optimization problems with parallel computational capability. In [8], adaptive MPC leverages multiple approximated linear models to simplify the calculation. Another approach is to achieve geometric control [9], based on a Lie group framework, to exploit

Y. Dong, Z. Xu, T. Lazouski and M. Ghaffari are with the University of Michigan, Ann Arbor, MI 48109, USA.

S. Teng is with the University of California, Berkley, CA 94709, USA.

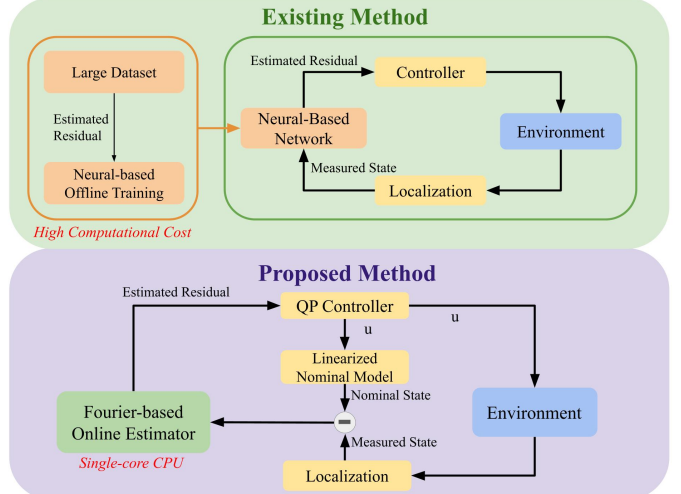


Fig. 1: Our method employs Fourier features to estimate the residual in an online manner and can be implemented efficiently on a single-core CPU. In contrast, prior online approaches rely on neural networks that require pre-training on large datasets.

symmetry in the problem. In this concept, Lie Algebraic MPC (Lie-MPC) is proposed [10], and applied on ASV [11]. Lie-MPC reduces computation time, making online learning for non-linear hydrodynamics applicable to ASV.

In parallel, several online learning methods have been proposed. In [12], a neural network-based adaptive module is incorporated into a model-based controller to compensate for large wave forces. In [13], the Deep Neural Network (DNN) is first trained offline to learn the model dynamics, then it is updated online to fit unknown disturbances. Similarly, in [14], a DNN is used to learn the system dynamics, and an Extended State Observer (ESO) measures error and makes up for residual dynamics estimation in the kinematic control law.

However, these neural-network approaches generally require GPU resources for offline pre-training on large datasets, which increases computational cost. Moreover, like in [14], the online-learning pipeline is used to directly change the system dynamics, making it difficult to generalize across different system setups. In [15], all disturbances are unified into a single locally Lipschitz term within the MPC dynamics and estimated through feature-based modeling. While this approach has been demonstrated on aerial vehicles and shown to reduce computational burden, its applicability to ASVs and its interaction with a Lie-MPC controller remain unexplored.

To mitigate the research gap, the main contributions of this work are as follows:

- 1) **A real-time online learning framework for MPC on ASVs.** We propose a novel integration of Fourier-based

online learning with convex Lie algebraic MPC that enables real-time disturbance compensation using only a single CPU core.

- 2) **Bi-level feature extraction for efficient disturbance representation.** We develop a bi-level Fourier-based feature extraction method that identifies and retains the dominant components of disturbance dynamics.
- 3) **Validation across simulation and real-world domains.** The proposed controller is evaluated in a physics-based simulator and in real-world experiments.

The remainder of this paper is organized as follows. Section II provides the mathematical preliminaries. Section III presents the details of our proposed method. Experiments are presented in Section IV. Finally, Section V concludes the paper and discusses future studies.

## II. PRELIMINARIES AND MATHEMATICAL FORMULATION

This section provides a brief overview of the necessary mathematical background used in the developed approach.

### A. Dynamics on Lie Group

This section briefly introduces the rigid body dynamics on the Lie group  $SE(3)$ . For more backgrounds on matrix Lie groups, refer to [16]–[18].

Let  $\mathcal{G}$  be an  $n$ -dimensional matrix Lie group with its associated Lie algebra  $\mathfrak{g}$ . We define the following isomorphism

$$(\cdot)^\wedge : \mathbb{R}^n \rightarrow \mathfrak{g}, \quad (1)$$

that maps an element in the vector space  $\mathbb{R}^n$  to the tangent space of the matrix Lie group at the identity. Its inverse mapping is denoted as  $(\cdot)^\vee : \mathfrak{g} \rightarrow \mathbb{R}^n$ . Then, for any  $\phi \in \mathbb{R}^n$ , we define the exponential map as

$$\exp(\cdot) : \mathbb{R}^n \rightarrow \mathcal{G}, \quad \exp(\phi) = \exp_m(\phi^\wedge), \quad (2)$$

where  $\exp_m(\cdot)$  denotes the matrix exponential.

To describe the 3D rigid body motion of the vehicle, we represent the rotation by matrix  $R \in SO(3)$  and the position vector by  $p \in \mathbb{R}^3$  and have the full state as:

$$X = \begin{bmatrix} R & p \\ 0 & 1 \end{bmatrix} \in SE(3). \quad (3)$$

The tangent space at the identity,  $\mathfrak{se}(3)$ , consists of twist  $\xi \in \mathbb{R}^6$ , which is defined as the concatenation of the angular velocity  $\omega$  and the linear velocity  $v$  in the body frame:

$$\xi = \begin{bmatrix} \omega \\ v \end{bmatrix}, \quad \xi^\wedge = \begin{bmatrix} \omega^\wedge & v \\ 0 & 0 \end{bmatrix} \in \mathfrak{se}(3). \quad (4)$$

The adjoint map of  $SE(3)$  has the matrix representation:

$$\text{Ad}_X = \begin{bmatrix} R & 0 \\ p^\wedge R & R \end{bmatrix}, \quad \text{ad}_\xi = \begin{bmatrix} \omega^\wedge & 0 \\ v^\wedge & \omega^\wedge \end{bmatrix}, \quad (5)$$

where  $\text{Ad}_X$  describes the change of frame of Lie algebra, and  $\text{ad}_\xi$  is defined by  $\text{ad}_\xi \eta = [\xi, \eta]$  with  $[\cdot, \cdot]$  the Lie bracket.

### B. Dynamics of ASV in Fossen's model

We will use a 6-DOF motion equations based on Fossen's model [19] to describe the ASV, with the the prescribed Lie group's ordering of twist vector  $\xi = [\omega, v]$ . The dynamics

are represented in the body frame following the convention of Euler Poincare equation for single rigid body:

$$M_{RB}\dot{\xi} + C_{RB}(\xi)\xi + M_{AM}\dot{\xi}_r + C_{AM}(\xi_r)\xi_r + D(\xi_r)\xi_r + g(\eta) = \tau_c + \tau_{disturb}^{body} \quad (6)$$

with  $M_{(\cdot)}$  the mass matrix,  $C_{(\cdot)}$  the Coriolis matrix. The subscript  $RB$  refers to the rigid-body contribution, while  $AM$  means “added mass”, which represents the inertia of fluid accelerated by the vehicle motions.  $D(\xi_r)$  is the hydrodynamic damping (drag) matrix.  $g(\eta)$  is the hydrostatic restoring force and moment vector, and here we assume the vehicle to be neutrally buoyant, so the hydrostatic term  $g(\eta)$  becomes negligible.  $\xi_r = \xi - \xi_c$  is the relative twist with respect to the ocean current  $\xi_c$ .  $\tau_c$  is the six-dimensional control input from the propulsion system,  $\tau_{disturb}^{body}$  is the six-dimensional external disturbance transformed in the body frame.

The mass matrix corresponding to  $\xi$  is given by

$$M = \begin{bmatrix} M_{11} & M_{12} \\ M_{21} & M_{22} \end{bmatrix}, \quad M_{ij} \in \mathbb{R}^{3 \times 3}, \quad (7)$$

there the submatrices are defined as  $M_{11}$  is a positive definite inertia matrix in body frame,  $M_{12} = M_{21}^\top = -m r_g^\wedge$ , and  $M_{22} = mI_3$ , where  $r_g = [x_g, y_g, z_g]^\top$  denotes the position vector of the center of gravity expressed in the body-fixed frame.  $(\cdot)^\wedge : \mathbb{R}^3 \rightarrow \mathfrak{so}(3)$  denotes the wedge operator that maps a vector to its corresponding skew-symmetric matrix. The Coriolis matrix is given by

$$C(\xi) = \begin{bmatrix} -(M_{11}\omega + M_{12}v)^\wedge & -(M_{21}\omega + M_{22}v)^\wedge \\ -(M_{11}\omega + M_{12}v)^\wedge & 0 \end{bmatrix} \quad (8)$$

which is a skew-symmetric that represents the “inertial forces” in the vehicle dynamics. The damping matrix is given by

$$D(\xi_r) = -\text{diag}\left(\begin{bmatrix} K_p, M_q, N_r, X_u, Y_v, Z_w \end{bmatrix}^\top\right) - \text{diag}\left(\begin{bmatrix} K_{|p|p}|p|, M_{|q|q}|q|, N_{|r|r}|r|, \\ X_{|u|u}|u|, Y_{|v|v}|v|, Z_{|w|w}|w| \end{bmatrix}^\top\right) \quad (9)$$

The damping terms model hydrodynamic effects such as potential damping, skin friction, wave drift damping, vortex shedding, and lifting forces. Depending on the surge velocity, either linear or nonlinear damping terms dominate. For non-coupled motion, a diagonal damping structure can be assumed, simplifying the dynamics.

Combining (5) with (6), have the full dynamics

$$M\dot{\xi} = \text{ad}_\xi^\top M\xi + F = -C(\xi)\xi - D(\xi)\xi + \tau, \quad (10)$$

$$\begin{bmatrix} \dot{R} & \dot{p} \\ 0 & 0 \end{bmatrix} = \begin{bmatrix} R & p \\ 0 & 1 \end{bmatrix} \begin{bmatrix} \omega^\wedge & v \\ 0 & 0 \end{bmatrix}. \quad (11)$$

with  $F \in \mathfrak{se}^*(3)$  the external force in the body frame.

## III. METHODS

In this section, we

### A. Error-State Convex MPC

We develop a convex error-state MPC by linearizing the tracking error dynamics in the Lie algebra and learn the residual dynamics to compensate for the modeling error.

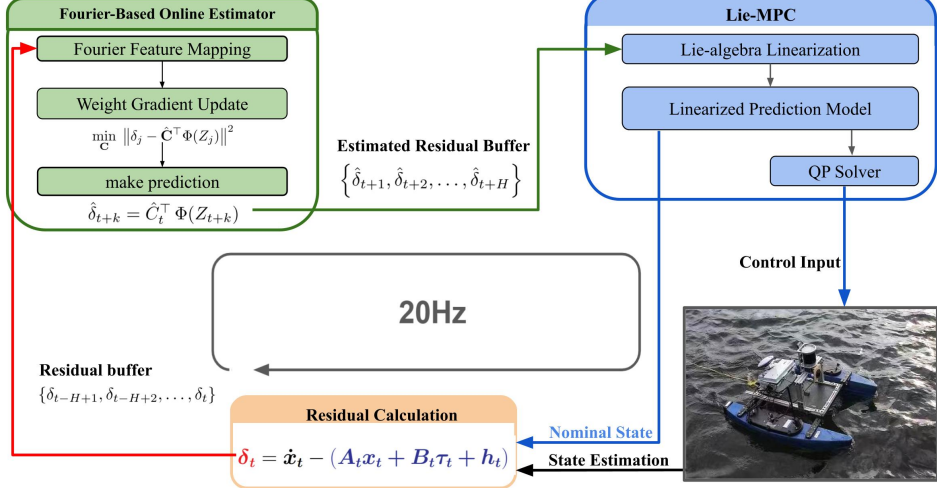


Fig. 2: This figure illustrates the overall pipeline. At each control cycle, a residual term is first computed by comparing the measured state derivative with the nominal dynamics model. A sliding buffer containing the most recent residual samples serves as the input to the Fourier-based online estimator. Then, the estimator updates the weight matrix to approximate this residual-history buffer and predicts a full horizon of future residual terms. These predicted residuals are then injected into the Lie-MPC, allowing the controller to account for upcoming disturbances over the entire planning horizon. In this manner, the proposed framework achieves real-time disturbance compensation without any weight pre-training and operates efficiently on resource-limited ASV platforms.

Let the desired trajectory be  $X_{d,t} \in \text{SE}(3)$ , and define the left-invariant error [20] on matrix Lie group as:

$$\Psi = X_{d,t}^{-1} X_t, \quad \dot{\Psi} = \Psi(\xi_t - A_{\Psi_t^{-1}} \xi_{d,t})^{\wedge}. \quad (12)$$

Using the first-order approximation  $\Psi_t \approx I + \psi_t^{\wedge}$ , we obtain the linearized error dynamics in Lie algebra:

$$\dot{\psi}_t = -ad_{\xi_{d,t}} \psi_t + \xi_t - \xi_{d,t}. \quad (13)$$

Linearizing the hydrodynamic model around  $\bar{\xi} = \xi_{d,t}$  yields:

$$M\dot{\xi} = H_t \xi + b_t + \delta_t^d + \tau, \quad (14)$$

where  $H_t$  and  $b_t$  are the Jacobian and residual terms derived from the first-order expansion of  $C(\xi)$  and  $D(\xi)$ , while  $\delta_t^d$  is derived from external hydrodynamic disturbance.

Define the system state  $x_t = [\psi_t, \xi_t]^{\top}$ , and the linearized hydrodynamic model becomes:

$$\dot{x}_t = A_t x_t + B_t \tau + h_t + \delta_t, \quad (15)$$

with each component defined by:

$$\begin{aligned} A_t &= \begin{bmatrix} -ad_{\xi_{d,t}} & I \\ 0 & H_t \end{bmatrix}, \quad B_t = \begin{bmatrix} 0 \\ M^{-1} \end{bmatrix}, \\ h_t &= \begin{bmatrix} -\xi_{d,t} \\ b_t \end{bmatrix}, \quad \delta_t = \begin{bmatrix} \delta_t^e \\ \delta_t^d \end{bmatrix}. \end{aligned} \quad (16)$$

Here,  $\delta_t^e$  represents the higher-order linearization residuals in the error-state dynamics, capturing higher-order terms neglected in the first-order approximation around  $\xi_{d,t}$ ,  $\delta_t^d$  denotes the external disturbances and unmodeled hydrodynamic effects.

For cost function, we first define the tracking output:

$$y_t = \begin{bmatrix} \psi_t \\ \dot{\psi}_t \end{bmatrix} = G_t x_t - d_t, \quad (17)$$

where

$$G_t = \begin{bmatrix} I & 0 \\ -ad_{\xi_{d,t}} & 0 \end{bmatrix}, \quad d_t = \begin{bmatrix} 0 \\ \xi_{d,t} \end{bmatrix}. \quad (18)$$

Then the cost function is formulated as:

$$J = y_N^{\top} P y_N + \sum_{k=1}^{N-1} (y_k^{\top} Q y_k + \tau_k^{\top} R \tau_k), \quad (19)$$

with  $P$ ,  $Q$ , and  $R$  the positive definite weighting matrices.

After discretization with step  $\Delta t$ , the MPC optimization problem becomes:

$$\begin{aligned} \min_{\tau_k} \quad & y_N^{\top} P y_N + \sum_{k=1}^{N-1} (y_k^{\top} Q y_k + \tau_k^{\top} R \tau_k) \\ \text{s.t.} \quad & x_{k+1} = A_k x_k + B_k \tau_k + h_k + \delta_k, \\ & x_0 = x_{\text{init}}, \quad \tau_k \in \mathcal{T}_k, \end{aligned} \quad (20)$$

where  $A_k = I + A_{t_k} \Delta t$ ,  $B_k = B_{t_k} \Delta t$ ,  $h_k = h_{t_k} \Delta t$ , and  $\delta_k = \delta_{t_k} \Delta t$ . The resulting QP can be efficiently solved using the OSQP solver.

---

#### Algorithm 1 Fourier Online MPC

---

**Require:** Total timesteps  $T$ ; MPC prediction horizon  $N$ ; feature map  $\Phi(\cdot)$ ; step size  $\eta$ ; regularizer  $\lambda$

- 1:  $x_1 \leftarrow [\psi_1, \xi_1]^{\top}$  ▷ Initialize system state
- 2:  $\hat{C}_t \leftarrow 0$  ▷ Initialize weight matrix
- 3:  $\hat{\delta}_{0|0} \leftarrow 0$  ▷ Initialize predicted residual
- 4: **for**  $t = 1, \dots, T$  **do**
- 5:    $\{\hat{\delta}_{t+k|t}\}_{k=1}^H \leftarrow \{\hat{C}_t^{\top} \Phi(Z_{t+k|t})\}_{k=1}^H$  ▷ Predict Residual
- 6:    $\tau_t \leftarrow \text{MPC}(x_t, \{\hat{\delta}_{t+k}\}_{k=1}^H)$  ▷ Solve (20)
- 7:    $\delta_t = \dot{x}_t - (A_t x_t + B_t \tau_t + h_t)$  ▷ Estimate residual
- 8:    $\ell_t \leftarrow (23)$  ▷ Compute loss
- 9:    $\hat{C}_{t+1} \leftarrow \hat{C}_t - \eta \nabla_{\hat{C}_t} \ell_t$  ▷ Update weights
- 10: **end for**

---

## B. Fourier-based Online Learning

At each time step  $t$ , we estimate the residual term  $\delta_t$  by comparing the measured and nominal state derivatives:

$$\delta_t = \dot{x}_t - (A_t x_t + B_t \tau_t + h_t), \quad (21)$$

where  $\dot{x}_t = (x_{t+1} - x_t)/\Delta t$  is obtained from discrete-time measurements using GPS and IMU fusion [21], and  $(A_t x_t + B_t \tau_t + h_t)$  is the nominal model from (15). The residual  $\delta_t = [\delta_t^e, \delta_t^d]^\top$  captures both internal linearization errors and external disturbances.

We approximate the residual by a Fourier basis evaluated on an input that concatenates the state  $x_t$  and time  $t$ :

$$Z_t = (x_t, t), \quad \hat{\delta}_t = C^\top \Phi(Z_t), \quad (22)$$

where  $\Phi(\cdot) : \mathbb{R}^{12} \times \mathbb{R} \rightarrow \mathbb{R}^d$  is the Fourier feature map that maps the time-dependent robot state to a  $d$ -dimensional feature. The coefficient matrix  $C$  is updated online using samples stored in a sliding buffer  $\mathcal{B}$ .

We use the most recent samples to compute a buffered loss with a temporal smoothness regularizer:

$$\ell_t = \frac{1}{N} \sum_{j=t-N+1}^t \left( \|\delta_j - \hat{\delta}_j\|^2 + \lambda \|\hat{\delta}_j - \hat{\delta}_{j-1}\|^2 \right), \quad (23)$$

We set  $\hat{\delta}_0 = 0$  for the smoothness term when  $j = 1$ . The optimization problem is formulated as

$$\hat{C} = \arg \min_C \ell_t \quad (24)$$

## C. Offline Bi-level Feature Extraction

Inspired by the Fourier-based nature of wave and wind disturbances [22], the features we use are all Fourier-based. However, directly using a large number of random Fourier features for disturbance estimation causes many of them fail to capture the dominant frequency components and spatial correlations of the residual term. To address this issue, we perform feature extraction to identify and retain components that contribute significantly to the residual representation. This reduces both the computational cost and the risk of overfitting while preserving model accuracy.

Each feature is represented as a sine–cosine pair obtained from a single variable  $z_{t,i}$  with a trainable frequency  $f_j$ :

$$\Phi(Z_t) = [\sin(f_j z_{t,i}), \cos(f_j z_{t,i})]_{i=1, \dots, d; j=1, \dots, m} \quad (25)$$

where  $d$  is the state dimension (12-dimensional state and 1-dimensional time) and  $m$  is the number of selected frequencies.

Let  $\{(Z_t, h_t)\}_{t=1}^T$  denote the dataset, where  $T$  is the total number of samples. We use a bi-level optimization to extract features, which alternates between amplitude and frequency updates. The problem is formulated as

$$\min_{\{f_j\}} \frac{1}{T} \sum_{t=1}^T \ell(h_t, \hat{C}(f) \Phi(Z_t)). \quad (26)$$

where

$$\hat{C}(f) = \arg \min_C \frac{1}{T} \sum_{t=1}^T \ell(h_t, C \Phi(Z_t)) + \lambda \|C\|_1. \quad (27)$$

## Algorithm 2 Offline Bi-level Feature Extraction

---

**Require:** Dataset  $\{(Z_t, h_t)\}_{t=1}^T$ ; initial amplitudes  $\hat{C}$ ; initial frequency set  $\{f_j\}_{j=1}^M$ ; feature map  $\Phi(\cdot)$ ; inner steps  $n_{\text{inner}}$ ; epochs  $N$ ; learning rate  $\eta$ ; regularization  $\lambda$

**Output:** Optimized Fourier feature map  $\Phi(\cdot)$

```

1: for epoch = 1 to  $N$  do
2:   Freeze  $\{f_j\}$ ; unfreeze  $\hat{C}$  ▷ Inner loop
3:   for  $k = 1$  to  $n_{\text{inner}}$  do
4:     for all  $(Z_t, h_t)$  in dataset do
5:        $\hat{h}_t \leftarrow \hat{C}^\top \Phi(Z_t)$ 
6:        $L_{\text{inner}} \leftarrow \|\hat{h}_t - h_t\|_1 + \lambda \|\hat{C}\|_1$  ▷ Compute loss
7:        $\hat{C} \leftarrow \hat{C} - \eta \nabla_{\hat{C}} L_{\text{inner}}$  ▷ Update weights
8:     end for
9:   end for
10:  Freeze  $\hat{C}$ ; unfreeze  $\{f_j\}$  ▷ Outer loop
11:  for all  $(Z_t, h_t)$  in dataset do
12:     $\hat{h}_t \leftarrow \hat{C}^\top \Phi(Z_t)$ 
13:     $L_{\text{outer}} \leftarrow \|\hat{h}_t - h_t\|_1$  ▷ Compute loss
14:     $\{f_j\} \leftarrow \{f_j\} - \eta \nabla_{f_j} L_{\text{outer}}$  ▷ Update weights
15:  end for
16: end for
17:  $\Phi(Z_t) \xleftarrow[\text{30 features}]{\text{PCA}} \Phi(Z_t)$  ▷ Extract Features

```

---

with  $\ell(\cdot, \cdot)$  denoting the L2 prediction loss. The inner optimization loop optimizes the amplitude parameters  $C$  with an  $\ell_1$  regularization that promotes sparsity, while the outer optimization loop adjusts the frequencies  $\{f_j\}$  to minimize the overall prediction error.

The inner optimization is a convex problem with respect to  $C$ , which guarantees a unique global optimum for fixed frequencies. We solve the overall bilevel objective using alternating minimization: fix  $\{f_j\}$  and update  $C$  (inner loop), then fix  $C$  and update  $\{f_j\}$  (outer loop). This alternating scheme adaptively learns both the most informative frequencies and their corresponding amplitudes. Even in the presence of Gaussian noise in the disturbance data, the convexity of the inner layer ensures convergence to a stable global minimum. The implementation is detailed in Algorithm 2.

## IV. EXPERIMENTS

### A. Experiment Setup

1) *Repetition Protocol:* This section involves tests under two scenarios: (i) the Virtual RobotX (VRX) simulator, and (ii) a real-world river experiment under wind. Tests in scenarios (i) are each repeated 10 times, with an initial position offset  $\Delta p_0 = [1.0\sqrt{u} \cos \theta, 1.0\sqrt{u} \sin \theta, 0]^\top \text{m}$ , where  $\theta \sim \mathcal{U}(0, 2\pi)$  and  $u \sim \mathcal{U}(0, 1)$ .

2) *Controller Tuning:* To reduce the coupling between observer and controller, we first approximate the dynamics with an LQR approximation. Given weighting matrices  $Q$ ,  $R$ , we compute  $P$  from the discrete-time algebraic Riccati equation (DARE)

$$P = A^\top P A = A^\top P B (R + B^\top P B)^{-1} B^\top P A + Q, \quad (28)$$

and set the stabilizing gain

$$K = (R + B^\top P B)^{-1} B^\top P A. \quad (29)$$

We tune weighting matrices  $Q$  and  $R$  based on eigenvalues of  $A - BK$ , avoiding complex conjugate pairs and ensuring the norm remains well below unity.

3) *Baselines*: We compare the performance of our method with those baseline methods: (1) **Nominal Lie-MPC**: the Lie-MPC framework without online learning [11]. (2) **L1 Adaptive-MPC**: the same MPC framework with an online L1-style disturbance-estimation module to calculate compensation based on residual dynamics as well. [23] (3) **PID**: A two-layer PID controller with an outer loop that computes the desired twist from pose errors, and an inner loop that tracks these references using two independent PID controllers:

$$v_x^{\text{ref}}, \omega_z^{\text{ref}} = f_{\text{outer}}(e_x, e_y, e_\psi), \quad (30)$$

$$u = f_{\text{inner}}(\text{PID}_v(v_x^{\text{ref}} - v_x), \text{PID}_\omega(\omega_z^{\text{ref}} - \omega_z)), \quad (31)$$

where  $u$  denotes the differential thrust command.

4) *Features for disturbance estimation*: After collecting disturbance and corresponding state variable in 10 rounds of simulation run in the Fossen model. We employ Algorithm 2 to extract 30 features, which are then used in multiple scenarios under various disturbances. The extracted features exhibit strong generalization capability.

5) *Performance metric*: We use the Root Mean Square Error (RMSE) as the performance metric for planar tracking. Since a random initial position error is introduced in each test, the RMSE is evaluated only after the ASV reaches a steady state to exclude the relatively large error at the beginning of each run. For instance, the RMSE is calculated over the second half of the path. For the selected segment  $\mathcal{K}$ , the trajectory-tracking RMSE for each run is

$$\text{RMSE} = \sqrt{\frac{1}{|\mathcal{K}|} \sum_{k \in \mathcal{K}} \| [x_k, y_k]^\top - [x_k^{\text{ref}}, y_k^{\text{ref}}]^\top \|_2}.$$

The values in the table are the mean and standard deviation of RMSE across repeated trials.

6) *Implementation details*: The experiments are conducted using two reference trajectories: (i) a zigzag path defined by a time-varying yaw rate  $\omega_z(t) = 0.1 \cos(t/100)$  with constant surge speed  $v_x = 0.5 \text{ m/s}$ , and (ii) a lawn-mower coverage pattern characterized by repeated straight segments ( $v_x = 0.5 \text{ m/s}$ ) and  $90^\circ$  turns executed at a turning rate  $\omega_z = 0.3 \text{ rad/s}$ . Both trajectories have a total duration of 128 s.

To incorporate the learned disturbances into the global MPC model, the estimated body-frame disturbance wrench  $\tau_t^{\text{body}}$  is transformed into the world frame via

$$\tau_t^{\text{world}} = \begin{bmatrix} R(X_t) & 0 \\ 0 & R(X_t) \end{bmatrix} \tau_t^{\text{body}}, \quad (32)$$

where  $R(X_t)$  is the rotation matrix corresponding to the ASV orientation. This operation assumes spatially uniform disturbances acting at the center of mass.

The algorithm configuration used across all experiments is summarized in Table I.

## B. Simulations in physics-based Virtual RobotX simulator

1) *System Setup*: We evaluate algorithm performance using the Virtual RobotX (VRX) simulator, which provides

TABLE I: Algorithm Configuration

Control Rate	Control Horizon $N$	step size $\eta$	Regularizer $\lambda$
50Hz	30	$10^{-4}$	$10^{-4}$

TABLE II: Trajectory-tracking RMSE for zigzag trajectory in VRX simulator.

Controller	0.0 m/s	1.0 m/s	2.0 m/s	3.0 m/s
PID	$2.901 \pm 0.068$	$3.115 \pm 0.044$	$3.932 \pm 0.175$	$8.798 \pm 0.334$
MPC	<b><math>0.093 \pm 0.002</math></b>	$0.193 \pm 0.051$	$0.809 \pm 0.013$	$1.441 \pm 0.710$
L1	$1.098 \pm 0.052$	$1.165 \pm 0.163$	$1.463 \pm 0.275$	$2.319 \pm 0.215$
<b>Ours</b>	$0.103 \pm 0.002$	<b><math>0.135 \pm 0.003</math></b>	<b><math>0.406 \pm 0.008</math></b>	<b><math>0.830 \pm 0.241</math></b>

a physics-based marine environment with realistic hydrodynamic and wind effects, as shown in Fig. 3. In simulations, the wave model and random wind seed are disabled for consistency, while the wind gain is fixed at 1 under the constant-speed option. A URDF model of the real-world ASV is imported into the simulator; the vessel has a mass of 28 kg and is actuated by two fixed parallel propellers with thrust limits of  $[-26, 50]$  N.

2) *Results*: As shown in Table II, Table III, Fig. 4, and Fig. 5, the proposed Online-MPC consistently achieves the lowest tracking error across all evaluated wind conditions and trajectories. For both the zigzag and lawn-mower trajectories, Online-MPC outperforms the nominal MPC, with the performance gap widening as wind speed increases, demonstrating improved robustness and disturbance-rejection capability under stronger environmental disturbances.

The PID controller exhibits the highest tracking error overall. Its performance degrades substantially with increasing wind speed, particularly in the zigzag trajectory, where the RMSE rises from approximately 2.9 at 0 m/s to nearly 8.8 at 3 m/s. Even in the simpler lawn-mower trajectory, PID maintains RMSE above 2.1 across all wind conditions, showing limited adaptability to disturbances. Similarly, the L1 adaptive MPC performs worse than nominal-MPC, possibly due to over-estimation under low disturbance. This pattern can also be observed in the lawn-mower trajectory, where L1 performs poorly under low wind disturbance but outperforms nominal-MPC in 3 m/s wind.

## C. Real-world Field Test

1) *System Setup*: As shown in Fig. 6, the ASV used is a modified Blue Robotics BlueBoat. We leverage an Nvidia



Fig. 3: The VRX environment.

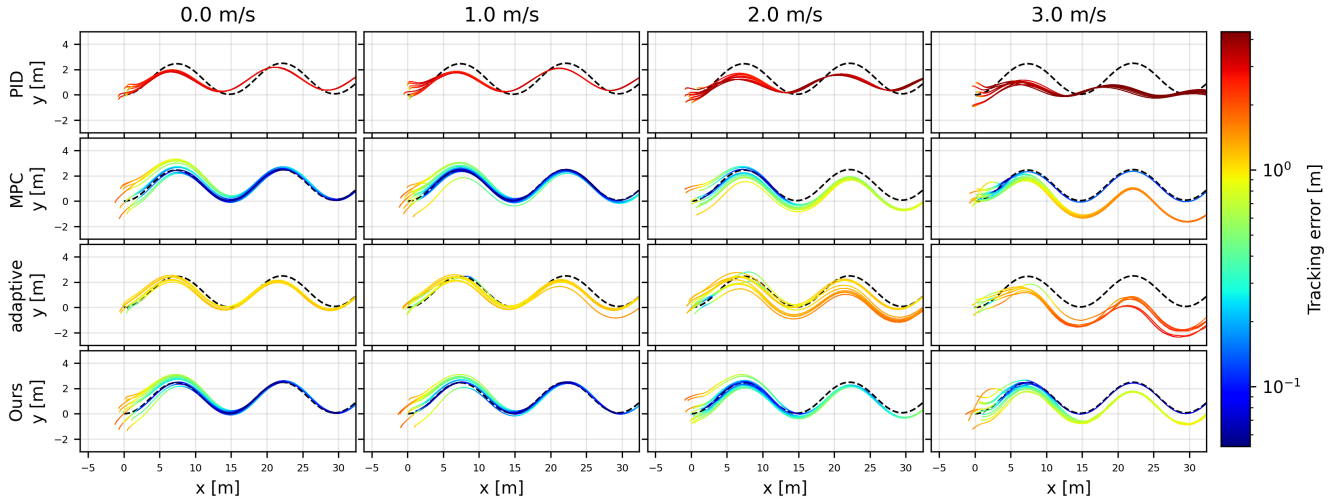


Fig. 4: Tracking performance of baselines and our method under different wind conditions in the VRX simulator.

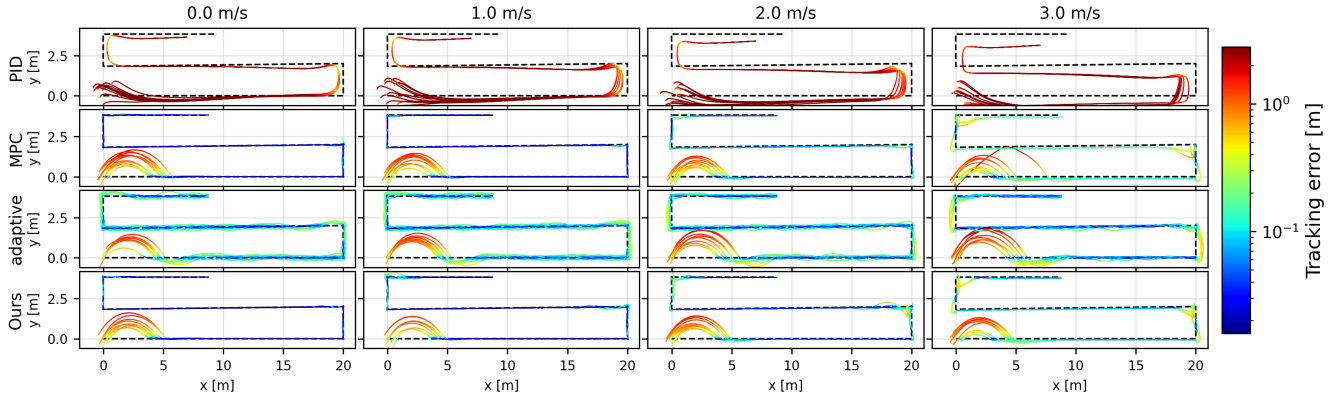


Fig. 5: Tracking performance of baselines and our method under different wind conditions in the VRX simulator.

TABLE III: Trajectory-tracking RMSE for lawnmower trajectory in VRX simulator.

Controller	0.0 m/s	1.0 m/s	2.0 m/s	3.0 m/s
PID	$2.131 \pm 0.001$	$2.137 \pm 0.001$	$2.159 \pm 0.002$	$2.209 \pm 0.002$
MPC	$0.022 \pm 0.001$	$0.022 \pm 0.001$	$0.046 \pm 0.001$	$0.131 \pm 0.000$
L1	$0.079 \pm 0.015$	$0.107 \pm 0.052$	$0.075 \pm 0.032$	$0.075 \pm 0.015$
<b>Ours</b>	$0.016 \pm 0.003$	$0.017 \pm 0.003$	$0.029 \pm 0.002$	$0.069 \pm 0.001$

Jetson Orin AGX to handle on-board computation. The vessel, together with a sensor suite, has a mass of 28 kg and is actuated by two fixed parallel propellers with thrust limits of  $[-26, 50]$  N.

Field experiments were conducted in the same environment multiple times. We launch the boat in three different directions, and separately test the performance of the proposed method and baseline Lie-MPC. External disturbances in the experiments include wind (approximately 1 m/s) and minor drag from the safety rope. These effects, together with internal linearization errors, provide a realistic evaluation of controller robustness.

2) *Results*: As shown in Table IV, Fig. 7, the proposed Online-MPC consistently outperforms the nominal MPC in zigzag trajectories. It achieves lower tracking errors and maintains stable operation under natural wind and current disturbances, demonstrating improved robustness and disturbance



Fig. 6: Real-world field test setup.

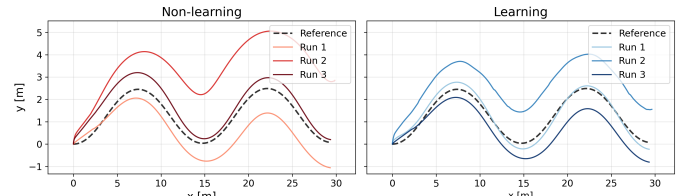


Fig. 7: The trajectories in the field test.

rejection capability in real-world conditions.

TABLE IV: Mean RMSE of trajectory tracking in field test.

Controller	RMSE (m)
MPC	$1.17 \pm 0.85$
<b>Ours</b>	<b><math>0.76 \pm 0.56</math></b>

## V. CONCLUSION

We presented an Online Learning-based Model Predictive Control (Online-MPC) framework for trajectory tracking under unknown disturbances. By integrating online residual compensation into MPC, the controller compensates for unmodeled dynamics such as wind and hydrodynamic variations in real time.

Both simulation and field experiments demonstrate that Online-MPC consistently outperforms the baselines, achieving lower tracking errors and greater robustness across diverse operating conditions. The results highlight the method's effectiveness and practicality as a low-cost method for autonomous surface vessels operating in uncertain and dynamic environments.

Further study may focus on deploying this algorithm on other ASVs in an environment with obvious waves or evaluating the algorithm on a more task-based measurement for common ASV missions.

## REFERENCES

- [1] E. Zereik, M. Bibuli, N. Mišković, P. Ridao, and A. Pascoal, "Challenges and future trends in marine robotics," *Annual Reviews in Control*, vol. 46, pp. 350–368, 2018. 1
- [2] Z. Liu, Y. Zhang, X. Yu, and C. Yuan, "Unmanned surface vehicles: An overview of developments and challenges," *Annual Reviews in Control*, vol. 41, pp. 71–93, 2016. 1
- [3] X. Gao and T. Li, "Dynamic positioning control for marine crafts: a survey and recent advances," *Journal of Marine Science and Engineering*, vol. 12, no. 3, p. 362, 2024. 1
- [4] Y. Cho, J. Han, and J. Kim, "Efficient COLREG-compliant collision avoidance in multi-ship encounter situations," *IEEE Transactions on Intelligent Transportation Systems*, vol. 23, no. 3, pp. 1899–1911, 2020. 1
- [5] A. Veksler, T. A. Johansen, F. Borrelli, and B. Realsen, "Dynamic positioning with model predictive control," *IEEE Transactions on Control Systems Technology*, vol. 24, no. 4, pp. 1340–1353, 2016. 1
- [6] E. I. Sarda, H. Qu, I. R. Bertaska, and K. D. Von Ellenrieder, "Station-keeping control of an unmanned surface vehicle exposed to current and wind disturbances," *Ocean Engineering*, vol. 127, pp. 305–324, 2016. 1
- [7] C. Liu, C. Li, and W. Li, "Computationally efficient MPC for path following of underactuated marine vessels using projection neural network," *Neural Computing and Applications*, vol. 32, no. 11, pp. 7455–7464, 2020. 1
- [8] A. S. Annamalai, R. Sutton, C. Yang, P. Culverhouse, and S. Sharma, "Robust adaptive control of an uninhabited surface vehicle," *Journal of Intelligent & Robotic Systems*, vol. 78, no. 2, pp. 319–338, 2015. 1
- [9] M. Ghaffari, R. Zhang, M. Zhu, C. E. Lin, T.-Y. Lin, S. Teng, T. Li, T. Liu, and J. Song, "Progress in symmetry preserving robot perception and control through geometry and learning," *Frontiers in Robotics and AI*, vol. 9, p. 969380, 2022. 1
- [10] S. Teng, D. Chen, W. Clark, and M. Ghaffari, "An error-state model predictive control on connected matrix Lie groups for legged robot control," in *Proc. IEEE/RSJ Int. Conf. Intell. Robots and Syst.* IEEE, 2022, pp. 8850–8857. 1
- [11] J. Jang, S. Teng, and M. Ghaffari, "Convex geometric trajectory tracking using Lie algebraic MPC for autonomous marine vehicles," *IEEE Robotics and Automation Letters*, vol. 8, no. 12, pp. 8374–8381, 2023. 1, 5
- [12] F. Tu, S. S. Ge, Y. S. Choo, and C. C. Hang, "Adaptive control for marine vessels against harsh environmental variation," *arXiv preprint arXiv:1909.13265*, 2019. 1
- [13] M. O'Connell, G. Shi, X. Shi, K. Azizzadenesheli, A. Anandkumar, Y. Yue, and S.-J. Chung, "Neural-fly enables rapid learning for agile flight in strong winds," *Science Robotics*, vol. 7, no. 66, p. eabm6597, 2022. 1
- [14] Z. Peng, F. Xia, L. Liu, D. Wang, T. Li, and M. Peng, "Online deep learning control of an autonomous surface vehicle using learned dynamics," *IEEE Transactions on Intelligent Vehicles*, vol. 9, no. 2, pp. 3283–3292, 2023. 1
- [15] H. Zhou and V. Tzoumas, "Simultaneous system identification and model predictive control with no dynamic regret," *IEEE Transactions on Robotics*, 2025. 1
- [16] B. C. Hall, "Lie groups, Lie algebras, and representations," in *Quantum Theory for Mathematicians*. Springer, 2013, pp. 333–366. 2
- [17] J. Sola, J. Deray, and D. Atchuthan, "A micro lie theory for state estimation in robotics," *arXiv preprint arXiv:1812.01537*, 2018. 2
- [18] F. Bullo and A. D. Lewis, *Geometric control of mechanical systems: modeling, analysis, and design for simple mechanical control systems*. Springer, 2019, vol. 49. 2
- [19] T. I. Fossen and O.-E. Fjellstad, "Nonlinear modelling of marine vehicles in 6 degrees of freedom," *Mathematical Modelling of Systems*, vol. 1, no. 1, pp. 17–27, 1995. 2
- [20] A. Barrau and S. Bonnabel, "The invariant extended Kalman filter as a stable observer," *IEEE Transactions on Automatic Control*, vol. 62, no. 4, pp. 1797–1812, 2016. 3
- [21] S. P. Singh, T. Lazouski, and M. Ghaffari, "GPS-DRIFT: Marine surface robot localization using IMU-GPS fusion and invariant filtering," *arXiv preprint arXiv:2507.02198*, 2025. 4
- [22] S. Lale, P. I. Renn, K. Azizzadenesheli, B. Hassibi, M. Gharib, and A. Anandkumar, "FALCON: Fourier Adaptive Learning and Control for Disturbance Rejection Under Extreme Turbulence," *npj Robotics*, vol. 2, no. 1, p. 6, 2024. 4
- [23] C. Cao and N. Hovakimyan, "Design and analysis of a novel L1 adaptive controller, Part I: control signal and asymptotic stability," in *Proc. Amer. Control Conf.*, 2006, pp. 3397–3402. 5